

# Adsorption and diffusion of strontium in simulated rock fractures quantified via ion beam analysis

T. OHE<sup>1</sup>, B. ZOU<sup>2</sup>, K. NOSHITA<sup>3</sup>, I. GOMEZ-MORILLA<sup>4,†</sup>, C. JEYNES<sup>4</sup>, P. M. MORRIS<sup>2</sup> AND R. A. WOGELIUS<sup>2,\*</sup>

<sup>1</sup> Energy, Engineering and Science Department, Tokai University, 1117 Kita Kaname, Hiratsuka-shi, Kanagawa 259-1292, Japan

<sup>2</sup> Williamson Research Centre for Molecular Environmental Science and School of Earth, Atmospheric and Environmental Sciences, University of Manchester, Oxford Road, Manchester M13 9PL, UK

<sup>3</sup> Energy and Environmental Systems Laboratory, Hitachi Ltd, 7-2-1 Omika, Hitachi-shi, Ibaraki 319-1221, Japan

<sup>4</sup> University of Surrey Ion Beam Centre, Guildford GU2 7XH, UK

[Received 16 December 2011; Accepted 3 June 2012; Associate Editor: Nicholas Evans]

## ABSTRACT

An experimental technique has been developed and applied to the problem of determining effective diffusion coefficients and partition coefficients of Sr in low permeability geological materials. This technique, the micro-reactor simulated channel method (MRSC), allows rapid determination of contaminant transport parameters with resulting values comparable to those determined by more traditional methods and also creates product surfaces that are amenable for direct chemical analysis. An attempt to further constrain mass flux was completed by detailed ion beam analysis of polished tuff surfaces (tuff is a polycrystalline polymineralic aggregate dominated by silicate phases) that had been reacted with Sr solutions at concentrations of  $10^{-5}$ ,  $10^{-3}$  and  $10^{-1}$  mol l<sup>-1</sup>. Ion beam analysis was carried out using beams of both protons (using particle induced X-ray emission and elastic backscattering spectrometry or EBS) and alpha-particles (using Rutherford backscattering spectrometry). The ion beam analyses showed that increased solution concentrations resulted in increased surface concentrations and that in the highest concentration experiment, Sr penetrated to at least 4 µm below the primary interface. The Sr surface concentrations determined by EBS were 0.06 ( $\pm 0.05$ ), 0.87 ( $\pm 0.30$ ) and 2.40 ( $\pm 1.0$ ) atomic weight % in the experiments with starting solution concentrations of  $10^{-5}$ ,  $10^{-3}$ , and  $10^{-1}$  mol l<sup>-1</sup>, respectively.

**KEY WORDS:** beam analysis (IBA), particle induced X-ray emission (PIXE), elastic backscattering spectrometry (EBS), Rutherford backscattering spectrometry (RBS), strontium.

## Introduction

RETENTION of radionuclides by geological materials is an important but often poorly constrained process (Seitz *et al.*, 1987). Measuring diffusive flux in fluid–rock systems is difficult due to the extremely slow rates of diffusion and generally low solute concentrations. However, diffusive

flux is expected to be an important mass transport process in radioactive waste repositories and therefore estimates of the diffusive flux of contaminant radionuclides are critical. Thus two obstacles exist in making such measurements: (1) conventional experiments need to be run over long periods of time under stable conditions; and (2) the analysis of adsorbed or precipitated contaminants must be able to determine low concentrations ideally with spatial resolution.

Interaction between the rock matrix and dissolved radionuclides can be characterized using the effective diffusion coefficient ( $D_e$ ) and the distribution coefficient ( $K_d$ ). Previous labora-

\* E-mail: roy.wogelius@manchester.ac.uk

† Current address: Technische Universität Dresden, Institut für Strömungsmechanik, Lehrstuhl für Magnetofluidynamik, 01062 Dresden, Germany

DOI: 10.1180/minmag.2012.076.8.33

tory scale experiments have been completed along with a theoretical analysis of the results in order to quantify the values of these coefficients (Skagius and Neretnieks, 1988). Despite their utility, certain limitations exist in the case of standard lab-scale diffusivity determinations. Firstly, the conventional technique is relatively time-consuming and months are needed to complete the measurement, particularly for strongly sorbing nuclides (Skagius and Neretnieks, 1982; Tsukamoto and Ohe, 1991). Long elapse times cause difficulties in maintaining constant experimental conditions and thereby create the risk of large uncertainties. In addition, different sample geometries are typically used depending on the parameter to be determined, e.g. crushed samples may be used for determining  $K_d$  whereas intact samples may be used for determining  $D_e$ . The dependence of both  $K_d$  (Rancon, 1986) and  $D_e$  (Tsukamoto and Ohe, 1991) on size has been observed and therefore an additional correction due to differing sample geometry is required to maintain consistency between parameters.

Therefore a fast method has been developed, hereafter referred to as the micro-reactor simulated-channel method (MRSC), to determine both  $D_e$  and  $K_d$  simultaneously using non-crushed rock samples (Okuyama *et al.*, 2008). The concept of this method is similar to that of the micro-chemical reactor, which has a very thin fluid flow channel (10–200 µm) and has the advantage of increasing the rate of surface reactions because of the high surface area to liquid volume ratio. This feature enables us to make very fast determinations even in a small reactor volume.

In the experiments, an aqueous fluid containing dissolved Sr has been pumped through a simulated rock fracture. Strontium is an expected radioactive contaminant in many nuclear waste repository scenarios, in particular the  $^{90}\text{Sr}$  isotope is the radioisotope of concern and has a half-life of 28.90 years. For convenience in these experiments we have used non-radioactive Sr. A solution bearing Sr as a proxy for radioactive contaminants has been forced through the simulated channel (or fracture) created between two polycrystalline wafers. Solute concentration was monitored as a function of time; Sr concentrations in the effluent were decreased relative to the inlet solution, and hence a quantity of Sr remained attached to the solids within the reactor. Concentrations remaining behind are much higher than would be predicted from simple surface adsorption onto the exposed wafers, and hence it is postulated that

some Sr has diffused into the boundaries between the grains that compose the polycrystalline wafers.

Therefore in order to determine the Sr inventory in the near surface of the solid interface, we developed an analytical regimen that included ion beam techniques. In particular, this approach was developed for the following two reasons. (1) It allowed us to take advantage of the extremely low background radiation levels at the  $\text{SrK}\alpha$  energy in particle induced X-ray emission (PIXE) analysis in order to accurately quantify Sr taken up by mineral surfaces in the micro-reactor experiments (Wogelius *et al.*, 1992, 1997). (2) We were able to use the depth profiling capability of elastic (non-Rutherford) backscattering spectrometry (EBS) and Rutherford backscattering spectrometry (RBS) to non-destructively constrain diffusion profiles below the surface. The distinction between RBS and EBS is solely in the applicable scattering cross-sections, which for RBS can be derived analytically from the Coulomb potential (Gurbich, 2010).

Our detailed approach involved preliminary analysis by environmental scanning electron microscope (ESEM) to determine grain morphology and check that levels of Sr were indeed enhanced after reaction. Samples were then to be analysed via PIXE with simultaneous EBS measurements. The EBS measurement was then repeated using alpha particles (RBS) in an attempt to give a fully constrained concentration depth profile with improved elemental resolution. Results were intended to give constraints on the grain boundary diffusion coefficients and total mass transfer into the solid matrix under our experimental conditions.

## Experimental materials and methods

### *Micro-reactor with simulated channel*

The new apparatus consists of an injection syringe pump, a reaction unit, an auto sampler, and a drainage tank (Fig. 1a). Rock samples were a natural tuff known as Itaya clinoptilolite (Iijima, 1980). All specimens were cut parallelepipeds, with dimensions of  $30 \times 20 \times 3$  mm, and the surfaces smoothed with abrasive paper (#200; Sankyo Rikagaku). The side edge surfaces were then coated with an epoxy resin to avoid evaporation of the test solution during experiments. The micro fluid channel was constructed using a fluoroplastic spacer. The reactor was connected with inlet and outlet ports (diameter 0.5 mm) for the injection or drainage of

## RETENTION OF RADIONUCLIDES BY GEOLOGICAL MATERIALS

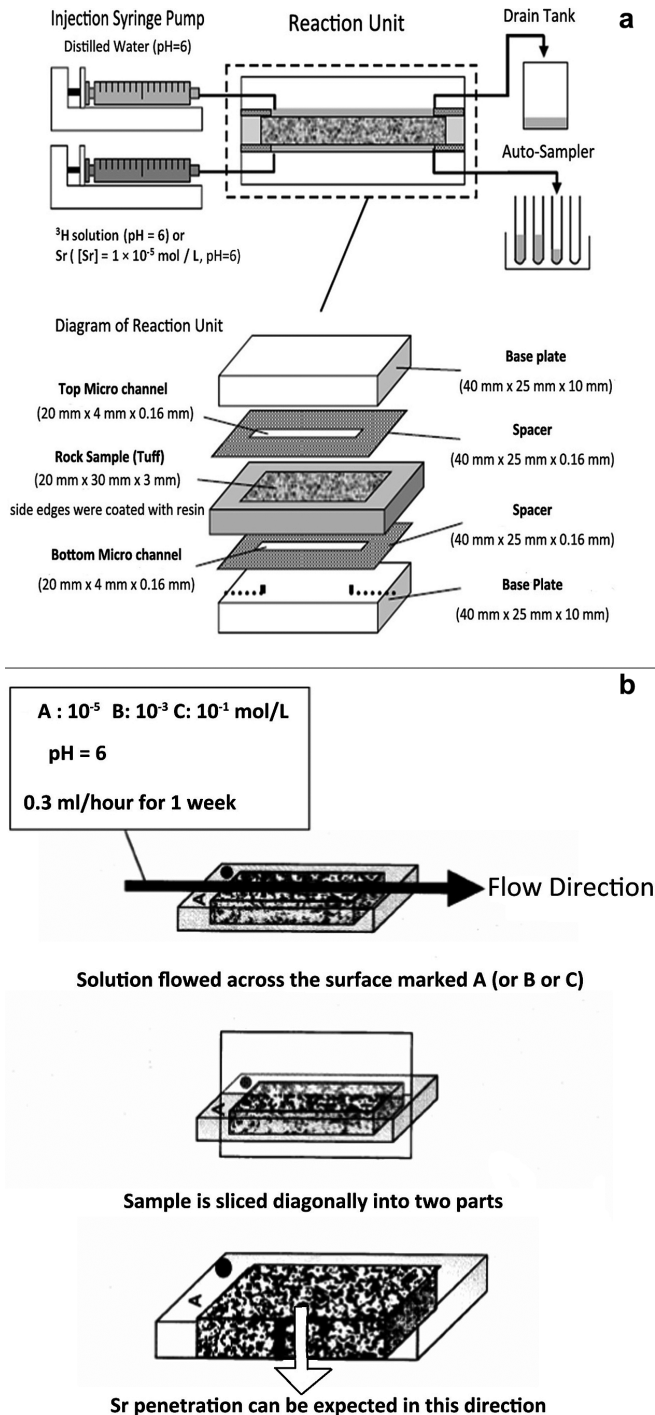


FIG. 1. (a) Experimental setup of the micro-channel reactor (Okuyama *et al.*, 2008). (b) Details of sample preparation for ion beam analysis. One face of the micro-channel was chosen for analysis after reaction. The sample was sliced longitudinally and then analysed with the incident beam parallel to the diffusion direction.

strontium-bearing solutions or distilled water. A test without the rock sample in place was carried out to verify that the surfaces of the fluoroplastic spacers and base plates were non-reactive.

Intact rock samples were cut and sized, then water-saturated in distilled water under a vacuum for 24 h prior to the experiments. A series of experiments was carried out at a constant flow rate of  $8.3 \times 10^{-11} \text{ m}^3 \text{ s}^{-1}$ . The accuracy of the measurements was better than 5%. The experimental apparatus was assembled in a glove box and all the experiments were performed at  $25 \pm 2^\circ\text{C}$ . Diffusive flux is perpendicular (normal) to the fluid–rock interface whereas advective flux is along the axis of the channel, normal to diffusion. Figure 1b indicates how samples were prepared for ion beam analysis. The inlet side was marked with a black dot and the sample was cut longitudinally. Analyses presented here were of the top surface, that is, the surface that had been directly in contact with the aqueous solution.

#### *Ion beam analysis analytical details*

The PIXE and RBS analyses were completed at the Ion Beam Centre, University of Surrey. A 2 MV tandem accelerator (Simon *et al.*, 2004) was used to produce the incident proton beam. The PIXE and EBS(H) used a beam of 2.5 MeV protons operating at 0.2 nA current. The resulting spectra were measured simultaneously for each area analysed. Detection of X-rays was by energy-dispersive spectroscopy (EDS) via a Si(Li) detector at either 30 or 60 mm distance with a 130  $\mu\text{m}$  Be filter placed between sample and detector to suppress low energy background. The sample-normal to detector angle was  $45^\circ$  and the beam spot was approximately  $3 \times 3 \mu\text{m}$ . The PIXE precision was  $\sim 1\%$  of the reported value except for Al, where the precision was  $\sim 10\%$  (unless otherwise noted). In the case of the backscattered proton signal, the detector surface area was  $150 \text{ mm}^2$  and the detector distance was 50 mm, giving a solid angle of 60 mSr. The scattering angle was  $150^\circ$ . Subsequent RBS( $\alpha$ ) measurements used a 1.554 MeV beam using two detectors with scattering angles of  $148.2^\circ$  ('IBM' geometry) and  $172.8^\circ$  ('Cornell' geometry) and solid angles of 6.5 and 1.25 mSr, respectively. The beam current was  $\sim 10$  nA and the nominal beam size (normal incidence) was 1 mm. The RBS errors in both cases are  $\sim 5\%$  for Si, O, and C;  $\sim 20\%$  for Ca, Fe, Al;  $\sim 40\%$  for Sr, Ba, K, and Na (unless otherwise noted).

Samples were attached to aluminium stubs by the epoxy enclosures and analysed under vacuum ( $1 \times 10^{-5}$  atm). The total charge (Q) and detector dead time were recorded and used in the calculation algorithms. The PIXE/EBS analysis was done using *Dan32* (Grime, 1996) and used the *GUPIX* code as a PIXE calculator (Blauw *et al.*, 2002). The RBS analysis was done using the *DataFurnace* code (Jeynes *et al.*, 2003). This practice of analysing multiple IBA datasets self-consistently has been recently reviewed in Jeynes *et al.* (2012).

#### *Environmental scanning electron microscopy and X-ray diffraction*

The energy dispersive spectrometry (EDS) analysis was performed with an ESEM using 20 kV accelerating voltage,  $32^\circ$  take off angle and 20% deadtime, with 0.2 Torr pressure in the column. The XRD was completed in a standard powder diffractometer using  $\text{CuK}\alpha$  radiation and a scan speed of  $1^\circ$  per minute with an angular resolution of  $0.02^\circ$ .

#### *Starting material*

The dominant mineral phases in the material were clinoptilolite (44–48 wt.%) and mordenite (10–43 wt.%) with quartz, opal and plagioclase also reported (Takasaka *et al.*, 1989). Figure 2 shows an XRD pattern of the starting material along with a comparison to two standard reference powder patterns. An excellent match exists between the clinoptilolite reference pattern and the sample used in these experiments. The stoichiometry of the clinoptilolite reference patterns is  $\text{Na}_{4.24}\text{K}_{0.28}\text{Ca}_{1.8}\text{Mg}_{0.16}\text{Al}_{8.16}\text{Si}_{27.84}\text{O}_{72.24.88}\text{H}_2\text{O}$  (79-1461). The reference pattern stoichiometries can be compared to the ideal stoichiometry as reported in Deer *et al.* (1992):  $(\text{Na},\text{K})_6[\text{Al}_6\text{Si}_{30}\text{O}_{72}] \cdot 24\text{H}_2\text{O}$ . The resultant RBS spectra also allowed us to calculate stoichiometries for comparison to these reference materials as presented below. In addition the XRD data indicated that a significant amount of quartz was present in the starting material (accounting for the peak at  $55^\circ 2\theta$ ,  $d = 1.6695 \text{ \AA}$ ).

#### *Reactant fluids*

Three experiments were completed at different dissolved Sr concentrations. We designate these simply as: (1) sample A, reacted with  $10^{-5} \text{ mol l}^{-1}$

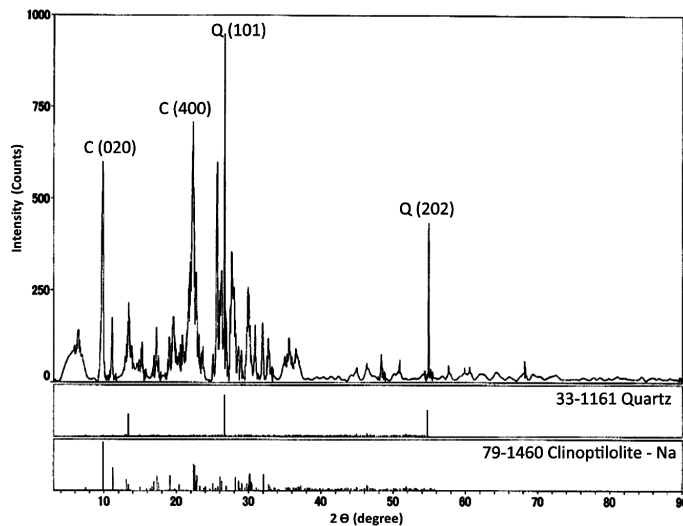


FIG. 2. The starting material XRD analysis showing the presence of clinoptilolite (C), a zeolite and quartz (Q). Miller indices for diagnostic peaks are labelled.

Sr solution; (2) sample B, reacted with  $10^{-3}$  mol l<sup>-1</sup> Sr solution; and (3) sample C, reacted with  $10^{-1}$  mol l<sup>-1</sup> Sr solution.

Two different samples were prepared for sample B: one for the MRSC experiment alone (sample B1) and the other both for the MRSC experiment and later beam analyses (sample B2). A stock solution of Sr was prepared by dissolving reagent grade SrCl<sub>2</sub> into deionized water. The solution pH was then adjusted to 6.0 by addition of either HCl or NaOH. Deuterated water (30 wt.%) as a non-sorbing solute tracer was included for sample B1. The deuterium concentrations in the outlet were determined by visible light absorption spectroscopy as a function of time (Okuyama *et al.*, 2008).

### Numerical analysis

In the following calculations, both advection and diffusion in the micro-channel were considered but only diffusion was considered for the rock matrix because its hydraulic conductivity is very small compared to that of the micro fluid channel. The micro channel was modelled as a hollow cylindrical tube in order to apply a radially symmetric computational approach, and the rock sample was regarded as a hollow cylinder mounted on this tube. The equation of the system was expressed as the one-dimensional diffusion-advection equation for the micro fluid

channel coupled with the matrix diffusion equation in two-dimensional cylindrical coordinate system. The governing equations were thus formulated as follows (Sudicky and Frind, 1982).

For the micro flow channel (0xL):

$$\left\{ 1 + \frac{K_c}{b} \right\} \frac{\partial C(x, t)}{\partial t} = D_L \frac{\partial^2 C(x, t)}{\partial x^2} - U_X \frac{\partial C(x, t)}{\partial x} + \frac{D_e}{b} \cdot \frac{\partial C_m(x, r, t)}{\partial r} \Big|_{r=R_a} \quad (1)$$

For the rock matrix ( $R_a \leq r \leq R_b$ ,  $0 \leq x \leq L$ ):

$$\varepsilon \left( 1 + \frac{\rho_d \cdot K_d}{\varepsilon} \right) \frac{\partial C_m(x, r, t)}{\partial t} = D_e \frac{\partial^2 C_m(x, r, t)}{\partial r^2} + \frac{1}{r} \frac{\partial}{\partial r} \left( D_e r \frac{\partial C_m(x, r, t)}{\partial r} \right) \quad (2)$$

where  $C(x, t)$  is the Sr concentration in the micro fluid channel (mol m<sup>-3</sup>);  $C_m(x, r, t)$  is the Sr concentration in the pore water of the rock matrix (mol m<sup>-3</sup>);  $r$  is the radial distance from the surface of the micro channel (m);  $x$  is the longitudinal distance from the injection point (m);  $t$  is the elapsed time (s);  $U_X$  is the flow velocity in the micro channel (m s<sup>-1</sup>);  $D_L$  is the longitudinal dispersion coefficient (m<sup>2</sup> s<sup>-1</sup>);  $D_e$  is the matrix diffusion coefficient (m<sup>2</sup> s<sup>-1</sup>);  $\varepsilon$  is the porosity of the rock (dimensionless);  $\rho_d$  is the density of the rock (kg m<sup>-3</sup>);  $b$  is the depth of the

micro channel (m);  $K_d$  is the sorption coefficient onto the rock matrix ( $\text{m}^3 \text{ kg}^{-1}$ );  $K_c$  is the surface sorption coefficient ( $\text{m}^3 \text{ m}^{-2}$ );  $L$  is the length of the rock sample and the micro channel (m);  $H$  is the height of the rock sample (m);  $W$  is the width of the rock sample (m);  $R_a$  is the inner radius of the hollow cylindrical rock sample (m); and  $R_b$  is the outer radius of the hollow cylindrical rock sample (m).

The initial concentration conditions were set equal to zero and a constant concentration boundary condition at the inlet was assumed. The conditions at both right and left ends of the sample were assumed to be a reflection boundary and then equations 1 and 2 are solved by using the finite control volume method (Patankar, 1980). A Langmuir sorption isotherm for Sr was assumed as has been used for other clinoptilolites (Li *et al.*, 2002), thus the sorption coefficient may be derived by equation 3:

$$K_d = \frac{q}{C} = q_\infty \cdot \frac{K_L}{1 + K_L C} \quad \text{when } C \rightarrow 0 \quad (3)$$

where  $q$  is the sorption amount ( $\text{mol kg}^{-1}$ );  $C$  is the liquid phase concentration ( $\text{mol m}^{-3}$ );  $q_\infty$  is the maximum sorption amount ( $\text{mol kg}^{-1}$ ); and  $K_L$  is the Langmuir sorption coefficient ( $\text{m}^3 \text{ kg}^{-1}$ ).

The maximum sorption amount ( $q_\infty$ ) was set equal to the half of the cation exchange capacity (CEC) of a high grade sample (Takasaka *et al.*, 1989) because of the impurities found in the XRD analysis. The Langmuir sorption coefficient ( $K_L$ ) was determined from the results of the batch sorption experiments, which gave a  $K_d$  value of

$58.7 (\text{m}^3 \text{ kg}^{-1})$ . This figure is similar to that of another Japanese tuff (Akiba and Hashimoto, 1990). From this value,  $K_L$  was simply calculated from equation 3 as  $78.5 \text{ m}^3 \text{ mol}^{-1}$ .

## Results and discussion

### Breakthrough curves

The breakthrough curves both of  $\text{D}_2\text{O}$  and Sr are shown in Fig. 3. Remarkably different breakthrough patterns were observed because of the different sorption characteristics of  $\text{Sr}^{2+}$  and  $\text{D}_2\text{O}$  on the sample. The effective diffusion coefficient in the rock matrix ( $D_e$ ) of  $\text{D}_2\text{O}$  given by least squares fitting was  $1.2 \times 10^{-10} \text{ m}^2 \text{ s}^{-1}$ .

Papelis and Um (2003) reported the  $D_e$  of non-sorbing species Br in a tuffaceous core sample with similar porosity of 28.8% to be  $1.75 \times 10^{-10} \text{ m}^2 \text{ s}^{-1}$ . This value is quite similar to that of the present analysis for  $\text{D}_2\text{O}$ . However, it is difficult to obtain a reliable  $D_e$  value for Sr from the breakthrough curve because concentrations are low (near the detection limit). Instead, the diffusion coefficient of  $\text{Sr}^{2+}$  was calculated using equation 4 (van Brakel and Heertjes, 1974) which considers the geometric effect of the pores in the matrix. The calculated breakthrough curve of  $\text{D}_2\text{O}$  is depicted in Fig. 3 and the value of  $F$  is determined as 0.064 by equation 4:

$$D_e = \varepsilon \cdot FD_v = \varepsilon \cdot \left( \frac{D_{e,D}}{D_{v,D}} \right) D_v \quad (4)$$

where  $F$  is the formation factor;  $D_v$  is the diffusion coefficient of  $\text{Sr}^{2+}$  in free water;  $D_{e,D}$

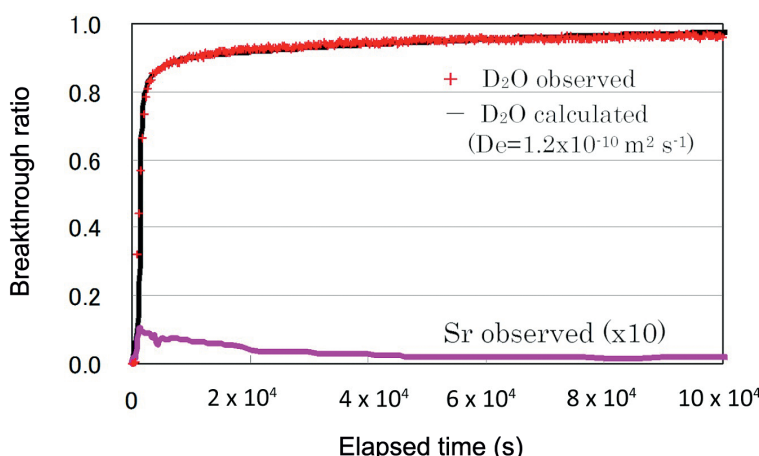


FIG. 3. Breakthrough curves of non-sorbing ( $\text{D}_2\text{O}$ ) and sorbing (Sr) tracers.

is the effective diffusion coefficient of D<sub>2</sub>O; and  $D_{v,D}$  is the self diffusion coefficient of D<sub>2</sub>O.

The properties used for the calculation of the breakthrough curves are summarized in Table 1. The matrix diffusion coefficient for Sr in this tuff is approximately a factor of two smaller than that for D<sub>2</sub>O.

### Analytical results

The ESEM maps and EDS analysis were completed on sample C showing that most grains were under 5 µm in length (in their

longest dimension). Along with the textural information, elemental mapping shows most regions have a constant Al/Si ratio of approximately ¼, consistent with clinoptilolite [different from quartz (0) or feldspar (½ to 1)], thus corroborating the XRD analysis. Compositional heterogeneity in the surface is quite high, however, and Fig. 4 shows a silicon map with small bright spots. These bright spots give an EDS pattern consistent with a pure SiO<sub>2</sub> phase which has been identified (and corroborated) via XRD analysis of the unreacted samples as quartz. The Sr was difficult to detect via ESEM-EDS.

TABLE 1. Sample properties used in the numerical analysis.

	Notation	Value	Unit	Remarks
Sample	length	$L$	$30 \times 10^{-3}$	m
	height	$H$	$3.1 \times 10^{-3}$	m
	width	$W$	$20 \times 10^{-3}$	m
Micro channel	length	$L$	$30 \times 10^{-3}$	m
	depth	$d$	0.16	m
	width	$W$	4	m
Hollow cylinder*	micro channel	$R_0$	$1.10 \times 10^{-3}$	m
	inner radius	$R_a$	$1.27 \times 10^{-3}$	m
	outer radius	$R_b$	$6.41 \times 10^{-3}$	m
Density	$\rho_d$	$1.18 \times 10^3$	$\text{kg m}^{-3}$	calculated by geometric volume and weight
Porosity	$\varepsilon$	0.32	—	measured by water displacement
Langmuir sorption coefficient	$K_L$	$7.85 \times 10^1$	$\text{m}^3 \text{mol}^{-1}$	determined by batch sorption experiments
Maximum sorption amount	$q_\infty$	$3.75 \times 10^{-1}$	$\text{mol kg}^{-1}$	derived from cation exchange capacity: 150 meq/100 g (Takasaka <i>et al.</i> , 1989)
Surface area at the interface	$S_C$	5.3	$\text{m}^2 \text{kg}^{-1}$	
Diffusion coefficient of Sr <sup>2+</sup> in free water	$D_v$	$7.92 \times 10^{-10}$	$\text{m}^2 \text{s}^{-1}$	(Yamaguchi <i>et al.</i> , 1993)
Self diffusion coefficient of D <sub>2</sub> O	$D_{v,D}$	$1.88 \times 10^{-9}$	$\text{m}^2 \text{s}^{-1}$	(Woolf, 1975)
Longitudinal dispersion coefficient	$D_L$	$7.92 \times 10^{-10}$	$\text{m}^2 \text{s}^{-1}$	dispersion effect is neglected
Flow velocity in the micro channel	$U_x$	$1.3 \times 10^{-4}$	$\text{m s}^{-1}$	corresponding volumetric flow rate is $5 \times 10^{-9} \text{ m}^3 \text{s}^{-1}$
Matrix diffusion coefficient	$D_{e,D}$	$5.06 \times 10^{-11}$	$\text{m}^2 \text{s}^{-1}$	calculated by equation 4

\* The surface area and the volume of the hollow cylinder were equal to those of micro channel or the rock specimen to simulate the mass flux and the mass conservation, simultaneously.

$$R_a = W/\mathbf{p}, R_b = (W \cdot H/\pi + \frac{d}{a})^{0.5}, R_0 + (R_a^2 - b \cdot H/\pi)^{0.5}$$

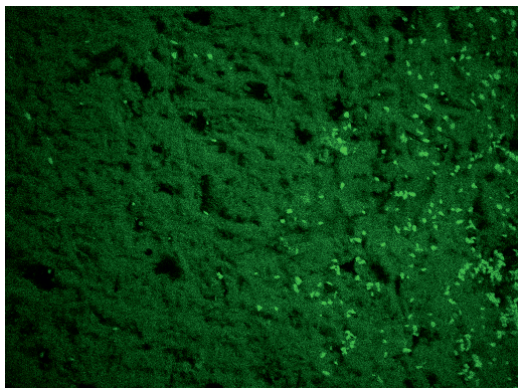


FIG. 4. The Si $K\alpha$  X-ray SEM map on sample C showing heterogeneity. The bright areas are quartz, verified by XRD and by EDS point analysis.

#### Particle induced X-ray emission

The PIXE analyses have an approximately  $10^3$  decrease in background relative to electron microprobe analysis as well as improved spatial resolution. The EBS with a proton beam (H-EBS) can be completed simultaneously with PIXE and allows depth resolution for flat surfaces plus direct analysis for light atoms such as carbon and oxygen. This means that mineral stoichiometry, metal concentration and element depth profiles can be determined at the same time and from the same point, line or area in a sample. This is of particular utility in studying trace-element profiles because it means that the depth profile of a specific component can be measured along with depth profiles of major elements (Grime *et al.*, 1993). In this way heterogeneities in the matrix both in the plane and normal to the surface plane may be accounted for and quantified. For comparison to the H-EBS data,  $\alpha$ -RBS using heavier alpha particles can typically give improved elemental resolution and hence improve depth profiling for specific components.

Samples A ( $10^{-5}$  mol l $^{-1}$ ), B ( $10^{-3}$  mol l $^{-1}$ ), and C ( $10^{-1}$  mol l $^{-1}$ ) were analysed. Sample C showed clear surface enrichment in Sr. Figure 5a shows a typical PIXE spectrum from this sample. For comparison, the Fig. 5b, show typical PIXE spectra taken from samples B and A, respectively. The major-element chemistry of all three analyses is essentially identical, as shown by the relative intensities of the K, Ca and Fe peaks. The Sr concentrations are completely different for each sample, however, as shown by the characteristic

peak intensities at approximately 14 keV. Quantitative analysis of Sr PIXE data obtained from area analyses ( $15 \times 15 \mu\text{m}$ ) for each sample are presented on Table 2, and indicate that sample C has a Sr loading of 1.61 at. wt.%, whereas sample A has levels that are below the detection limit. Although the absolute errors increase from A to C, the relative errors decrease as the concentration of Sr rises well above the detection limits for both the PIXE and EBS measurements.

The PIXE concentration maps were also used to check for Sr heterogeneity. Most of the recorded characteristic Sr intensity in sample A can be ascribed to elevated Sr concentrations in a few small plagioclase feldspar grains included within the starting material. A map and point analyses of a feldspar grain and of the surrounding nearby clinoptilolite are shown in Fig. 6. These analyses clearly show that small quantities of Sr are indeed contained by the plagioclase (which also has higher Ca levels than the clinoptilolite) within the starting material. This is not a volumetrically important phase in the tuff and the Sr concentrations are low (110 ppm), but this nonetheless needs to be accounted for when considering the Sr inventory of these samples. We also note that the Sr signal is homogeneous and relatively high over the entire surface area of sample C, and hence we assume that the Sr intensity is overwhelmingly due to surface adsorption in this case and is unaffected by Sr in the starting material. Sample B shows some degree of compositional heterogeneity for Sr.

The EBS analyses resolved the presence of Sr on the surfaces of all three samples. A calculated fit to the sample C spectrum is presented in Fig. 7a and gives a surface concentration of 2.4 wt.% Sr, with the profile showing that Sr has penetrated to a depth of at least 4  $\mu\text{m}$  below the sample surface. Using the bulk composition of the clinoptilolite reference material as a starting

TABLE 2. Sr concentrations (with  $2\sigma$  errors) determined at the surfaces of the samples.

Sr (wt.%)	A	B	C
PIXE	bld*	$0.59 \pm 0.01$	$1.61 \pm 0.02$
EBS (H)	$0.06 \pm 0.05$	$0.87 \pm 0.3$	$2.40 \pm 1.0$
RBS ( $\alpha$ )			$3.02 \pm 1.5$

\* Below the limit of detection.

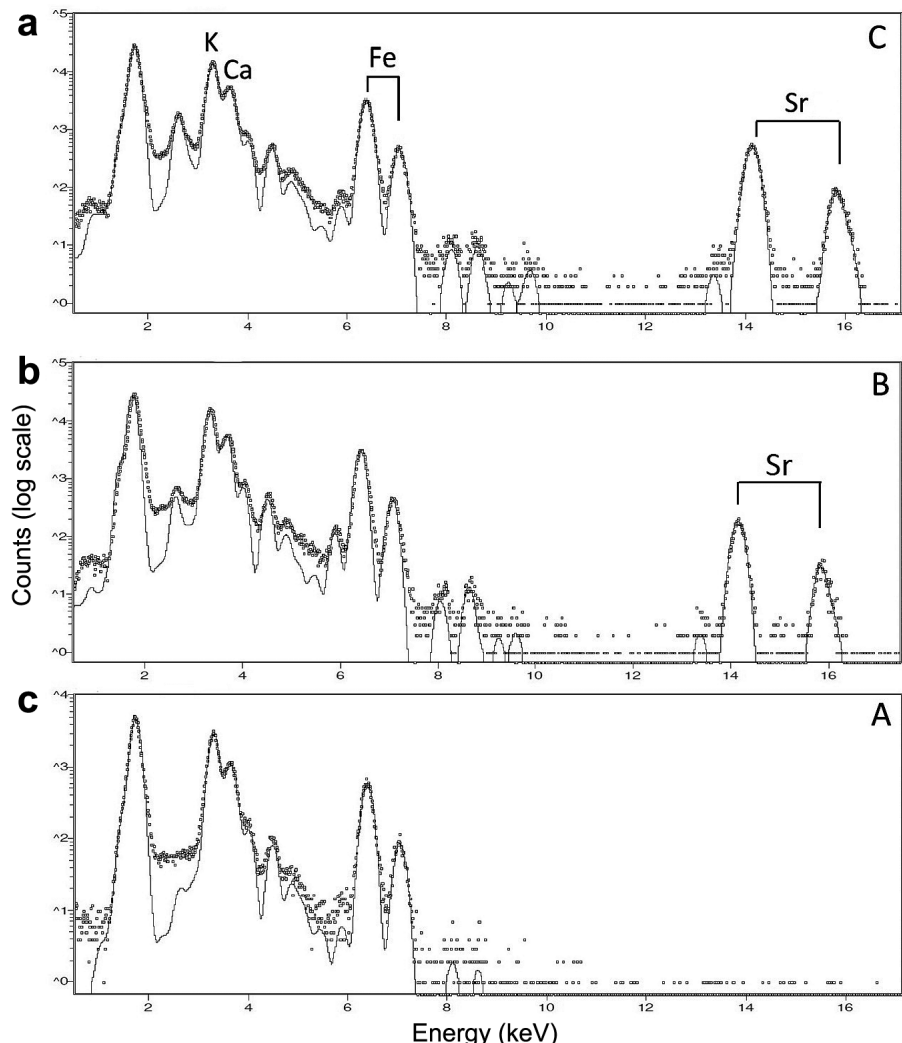


FIG. 5. The 2.5 MeV PIXE EDS analyses of samples A, B, and C. Note decreasing Sr intensity and virtually no background at the  $\text{SrK}\alpha$  energy.

point, the  $\alpha$ -RBS calculation not only gave results for Sr, but also showed surface contamination with carbon and refined the stoichiometry of the clinoptilolite to be  $\text{Na}_{3.4}\text{K}_{2.2}\text{Ca}_{0.1}\text{Fe}_{0.4}\text{Al}_{3.7}\text{Si}_{25.8}\text{O}_{72.5}\cdot24\text{H}_2\text{O}$ . This best fit stoichiometry is close to the reference pattern and gives us confidence that the H-EBS fit is robust. Figure 7*b,c* also presents the best fit calculations of the H-EBS data for samples B and A, respectively. Surface Sr was detected in both cases by this technique, although in the case of sample A these concentrations were barely above the detection limit (Table 2). Perhaps most

importantly, fits to the EBS and RBS data confirm that Sr has penetrated to at least 4  $\mu\text{m}$  below the surface of the tuff in samples B and C.

### Summary and conclusions

Table 3 presents a comparison of the concentrations of major and trace elements determined for the surface of the reacted sample C by the various analytical techniques employed in this study plus a reference composition for clinoptilolite taken from the literature. We note that all of the techniques employed were standardless. Given

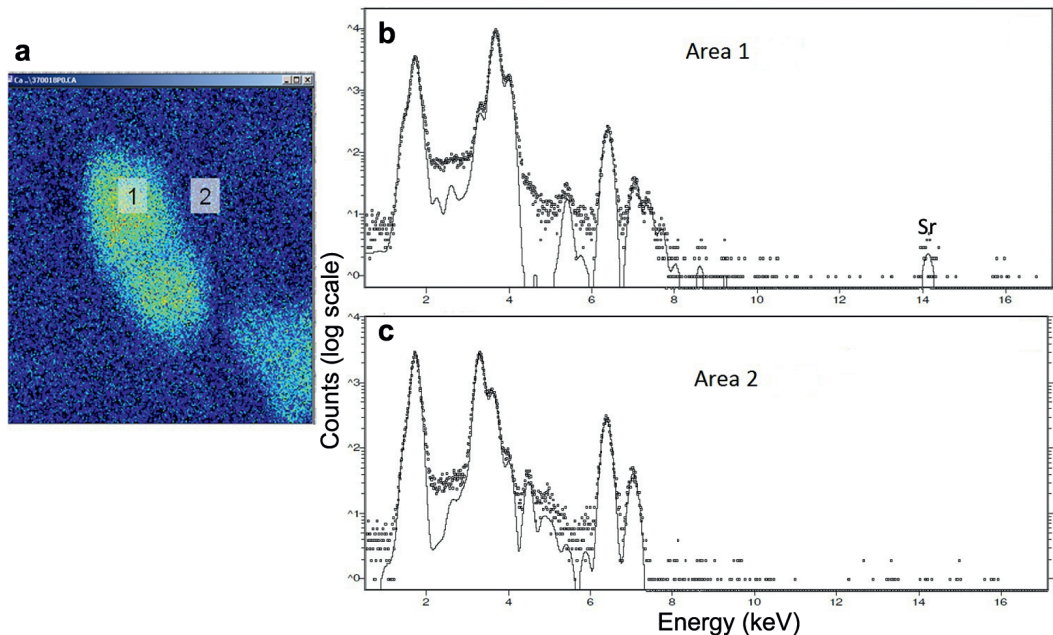


FIG. 6. Measurable Sr is apparently present in at least one of the starting mineral phases. (a) Sample A, 2.5 MeV PIXE Ca map: 150 × 150  $\mu\text{m}$ . (b) Area analysis (1) of high Ca area, plagioclase feldspar, reveals 110 ppm Sr. (c) Area 2, representative of the bulk of the sample, has no detectable Sr. Area analyses are 15 × 15  $\mu\text{m}$ .

the heterogeneities in the starting material some variability is expected, however the accuracy and precision for all of the major elements is extremely good, except the ESEM-EDS analysis for Sr. The ion beam techniques agree within error for the surface loading of Sr in this experiment, and this, along with the  $D_e$  and  $K_d$  values determined above, therefore allows us to

constrain surface loading and mass transfer for samples A, B and C.

A new technique, the micro-reactor simulated fracture method, was developed by adopting the concept of a micro chemical reactor for simultaneous determination of the diffusion coefficient and sorption coefficient of rock samples. The advantages of the new method

TABLE 3. Comparison of chemical analyses, sample C, element (wt.%).

	RBS (H)	RBS( $\alpha$ )	PIXE	ESEM-EDS	Reference*
Na	2.65				3.11
K	2.91	2.14	1.02	5.13	3.35
Ca	0.14		0.26	0.39	0.64
Fe	0.66	1.46	0.43	0.42	0.41
Al	3.41	6.79	7.75	5.34	7.02
Si	24.41	34.28	24.43	24.76	28.88
O	52.26	52.24		46.43	54.52
C	9.54			12.46	
Sr	2.40	3.02	1.61	6.89	0.03
Ba		0.07			0.09

\* Deer *et al.* (1992, page 527, Table 49, analysis 8. ESEM-EDS, average of three analyses except Sr, N = 2).

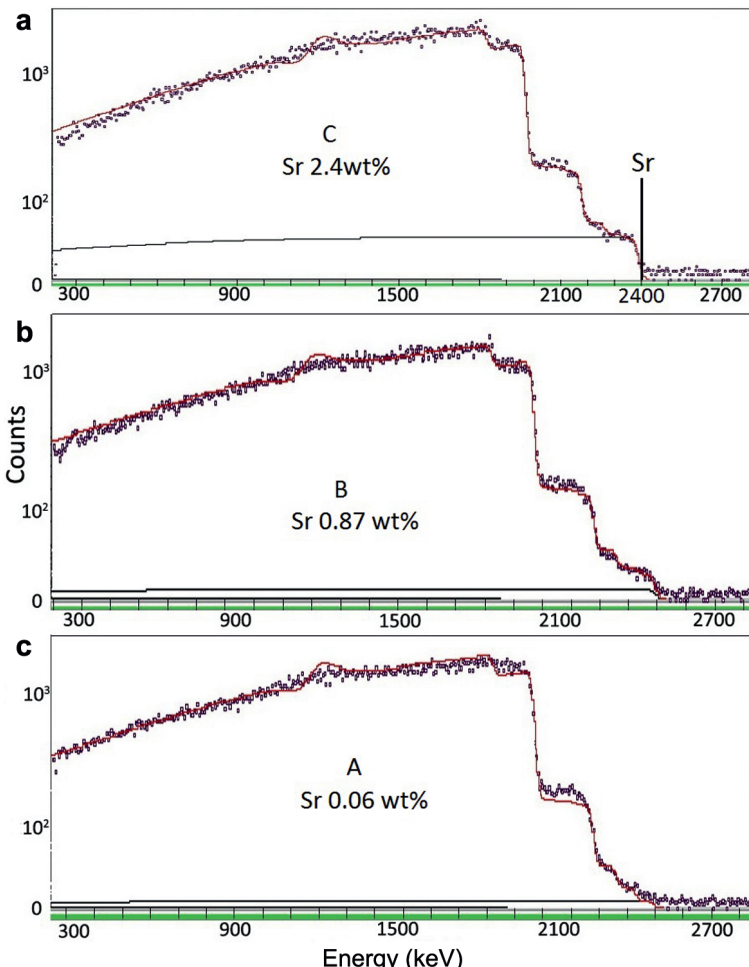


FIG. 7. Calculated fits to the 2.5 MeV H-EBS data. Major-element stoichiometry is roughly constant, but Sr decreases in order C > B > A. In samples B and C, width of Sr plateau indicates Sr has penetrated at least 4  $\mu\text{m}$ . Note the square root scale on the ordinate. Note also the  $^{28}\text{Si}(\text{p},\text{p})^{28}\text{Si}$  resonance at 2.08 MeV that is smeared out in the data by sample roughness.

were verified by comparing with conventional techniques. Strontium was chosen for the analyses and the breakthrough curves were obtained for a parallelepiped tuff sample. Good agreement was found between values obtained by the different methods within measurement errors. Furthermore, ion beam techniques were used to produce depth-resolved chemical analyses with low detection limits of reacted surfaces in order to fully constrain the inventory of Sr in the near surface of the reacted rock. It is clear that increased solution concentrations resulted in increased adsorbate density. The PIXE and EBS/RBS

easily quantified Sr at the surfaces, however grains such as those imaged in Fig. 6 greatly complicated the analysis and created a heterogeneous background. Future work should be aware of such complications. In particular, for Sr diffusion measurements with natural materials investigators need to be aware of the high concentrations of Sr associated with some feldspar and carbonate minerals. The RBS depth profiling verified that Sr penetrated deeply below the surface of the channel (approximately 4  $\mu\text{m}$ ), however high sample roughness precluded accurately resolved depth profiling. Granite or another

similar rock type that can be chemo-mechanically polished, with large crystals and well defined grain boundaries, will be used in future work.

## Acknowledgements

Both RAW and TO gratefully acknowledge EPSRC grant EP/D032210/1 to the University of Surrey Ion Beam Centre and the assistance of Drs Geoff Grime and Karen Kirkby; PMM was supported via a University of Manchester Research Associate position granted with the assistance of Prof. R.A.D. Pattrick; BZ is supported by the EPSRC/Diamond consortium. Financial support was also given by the Central Research Institute of the Electrical Power Industry of Japan.

## References

- Akiba, K. and Hashimoto, H. (1990) Distribution coefficient of strontium on a variety of minerals and rocks. *Journal of Nuclear Science and Technology*, **27**, 275–279.
- Blaauw, M., Campbell, J.L., Fazinic, S., Jaksic, M., Orlic, I. and Van Espen, P. (2002) The 2000 IAEA intercomparison of PIXE spectrum. *Nuclear Instruments and Methods in Physics Research*, **B189**, 113–122.
- Deer, W.A., Howie, R.A. and Zussman, J. (1992) *An Introduction to the Rock-Forming Minerals*, second edition. Pearson Education, Harlow, UK.
- Grime, G.W. (1996) The “Q factor” method: quantitative microPIXE analysis using RBS normalisation. *Nuclear Instruments and Methods in Physics Research*, **B109**, 170–174.
- Grime, G.W., Watt, F., Wogelius, R.A. and Jamtveit, B. (1993) Processing micro PIXE lines can data – studies of arsenic zoning in skarn garnets. *Nuclear Instruments and Methods in Physics Research*, **B77**, 410–414.
- Gurbich, A.F. (2010) Evaluated differential cross-sections for IBA. *Nuclear Instruments and Methods in Physics Research*, **B268**, 1703–1710.
- Iijima, A. (1980) Geology of natural zeolites and zeolitic rocks. *Pure and Applied Chemistry*, **52**, 2115–2130.
- Jeynes, C., Barradas, N.P., Marriott, P.K., Boudreault, G., Jenkin, M., Wendler, E. and Webb, R.P. (2003) Elemental thin film depth profiles by ion beam analysis using simulated annealing – a new tool. *Journal of Physics D: Applied Physics*, **36**, R97–R126.
- Jeynes, C., Bailey, M.J., Bright, N.J., Christopher, M.E., Grime, G.W., Jones, B.N., Palitsin, V.V. and Webb, R.P. (2012) Total IBA – where are we? *Nuclear Instruments and Methods in Physics Research*, **B271**, 107–118.
- Li, Z., Alessi, D. and Allen, L. (2002) Influence of quaternary ammonium on sorption of selected metal cations onto clinoptilolite zeolite. *Journal of Environmental Quality*, **31**, 1106–1114.
- Okuyama, K., Sasahira, A., Noshita, K. and Ohe, T.A. (2008) Method for determining both diffusion and sorption coefficients of rock medium within a few days by adopting a micro-reactor technique. *Applied Geochemistry*, **23**, 2130–2136.
- Papelis, C. and Um, W. (2003) *Evaluation of Cesium, Strontium, and Lead Sorption, Desorption, and Diffusion in Cores from Western Pahute Mesa, Nevada Test Site, Based on Macroscopic and Spectroscopic Investigation*. Department of Energy Publication No. 45187, DOE/NV/13609-16. US Department of Energy, Nevada, USA.
- Patankar, S.V. (1980) *Numerical Heat Transfer and Fluid Flow*. Taylor & Francis, London.
- Rancon, D. (1986) Influence of concentration distributions in solid medium on the assessment of radioelement distribution between the liquid and solid phases. Pp. 64–71 in: *Application of Distribution Coefficients to Radiological Assessment Models* (T.H. Sibley and C. Myttenaere, editors). Elsevier Applied Science, London.
- Seitz, M.G., Wogelius, R.A. and Flower, M.F. (1987) Nuclear waste elements slip through hydrothermally altered basalt. *Chemical Geology*, **64**, 109–119.
- Simon, A., Jeynes, C., Webb, R.P., Finnis, R., Tabatabian, Z., Sellin, P.J., Breese, M.B.H., Fellows, D.H., Van den Broek, B. and Gwilliam, R.M. (2004) The new Surrey ion beam analysis facility. *Nuclear Instruments and Methods in Physics Research*, **B219–B220**, 405–409.
- Skagius, K. and Neretnieks, I. (1982) Diffusion in crystalline rock. Pp. 509–518 in: *Scientific Basis for Nuclear Waste Management V* (V.W. Lutze, editor). Elsevier, Amsterdam.
- Skagius, K. and Neretnieks, I. (1988) Measurement of cesium and strontium diffusion in biotite gneiss. *Water Resources Research*, **24**, 75–84.
- Sudicky, E.A. and Frind, E.O. (1982) Contaminant transport in fractured porous media: analytical solutions for a system of parallel fractures. *Water Resources Research*, **18**, 1634–1642.
- Takasaka, A., Matsuda, Y. and Ito, H. (1989) Purification of Itaya zeolite on an industrial scale and its characteristics. *Nihon Kagakukai-Shi*, **3**, 621–627, [in Japanese].
- Tsukamoto, M. and Ohe, T. (1991) Intraparticle diffusion of cesium and strontium cations into rock materials. *Chemical Geology*, **90**, 31–44.
- Van Brakel, J. and Heertjes, P.M. (1974) Analysis of

## RETENTION OF RADIONUCLIDES BY GEOLOGICAL MATERIALS

- diffusion in macroporous media in terms of porosity, a tortuosity and a constrictivity factor. *International Journal of Heat and Mass Transfer*, **17**, 1093–1103.
- Wogelius, R.A., Fraser, D.G., Feltham, D. and Whiteman, M. (1992) Trace elements in dolomite: proton microprobe data and constraints on fluid compositions. *Geochimica et Cosmochimica Acta*, **56**, 319–334.
- Wogelius, R.A., Fraser, D.G., Grime, G.W. and Wall, G.R.T. (1997) Trace element and isotopic zonation in vein calcite from the Mendip Hills, UK, with spatial-process correlation analysis. *Geochimica et Cosmochimica Acta*, **61**, 2037–2051.
- Woolf, L.A. (1975) Tracer diffusion of tritiated heavy water (DTO) in heavy water ( $D_2O$ ) under pressure. *Journal of the Chemical Society, Faraday Transactions, I*, **72**, 1267–1273.
- Yamaguchi, T., Sakamoto, Y. and Senoo, M. (1993) Consideration on effective diffusivity of strontium in granite. *Journal of Nuclear Science and Technology*, **30**, 796–803.